Archival Report

Biological Psychiatry: CNNI

White Matter Indices of Medication Response in Major Depression: A Diffusion Tensor Imaging Study

Andrew D. Davis, Stefanie Hassel, Stephen R. Arnott, Jacqueline Harris, Raymond W. Lam, Roumen Milev, Susan Rotzinger, Mojdeh Zamyadi, Benicio N. Frey, Luciano Minuzzi, Stephen C. Strother, Glenda M. MacQueen, Sidney H. Kennedy, and Geoffrey B. Hall

ABSTRACT

BACKGROUND: While response to antidepressants in major depressive disorder is difficult to predict, characterizing the organization and integrity of white matter in the brain with diffusion tensor imaging (DTI) may provide the means to distinguish between antidepressant responders and nonresponders.

METHODS: DTI data were collected at 6 sites (Canadian Biomarker Integration Network in Depression-1 [CAN-BIND-1 study]) from 200 (127 women) depressed and 112 (71 women) healthy participants at 3 time points: at baseline, 2 weeks, and 8 weeks following initiation of selective serotonin reuptake inhibitor treatment. Therapeutic response was established by a 50% reduction of symptoms at 8 weeks. Analysis on responders, nonresponders, and control subjects yielded 4 scalar metrics: fractional anisotropy and mean, axial, and radial diffusivity. Region-of-interest analysis was carried out on 40 white matter regions using a skeletonization approach. Mixed-effects regression was incorporated to test temporal trends.

RESULTS: The data acquired at baseline showed that axial diffusivity in the external capsule, which overlaps the superior longitudinal fasciculus, was significantly associated with medication response. Regression analysis revealed further baseline differences of responders compared with nonresponders in the cingulum regions, sagittal stratum, and corona radiata. Additional group differences relative to control subjects were seen in the internal capsule, posterior thalamic radiation, and uncinate fasciculus. Most effect sizes were moderate (near 0.5), with a maximum of 0.76 in the cingulum-hippocampus region. No temporal changes in DTI metrics were observed over the 8-week study period.

CONCLUSIONS: Several DTI measures of altered white matter specifically distinguished medication responders and nonresponders at baseline and show promise for predicting treatment response in depression.

Keywords: Depression, Diffusion tensor imaging, Mixed effects regression, Multisite MRI, SSRI, Treatment response

https://doi.org/10.1016/j.bpsc.2019.05.016

In major depressive disorder (MDD), only about 60% of affected individuals respond to treatment with selective serotonin reuptake inhibitor (SSRI) antidepressants, and even fewer go into remission (1). Predicting treatment response is difficult, leading to delayed commencement of secondary treatments that can cause increased illness duration and possible mortality. The ability to characterize brain differences between medication responders and nonresponders using magnetic resonance imaging may lead to improved patient care and prognosis.

Evidence from functional imaging research has linked the altered emotional and cognitive processing in depression to an imbalance between overreactive subcortical limbic networks and underreactive prefrontal-limbic networks (2–5). Further, evidence has suggested that antidepressants correct this imbalance, normalizing corticolimbic functional activity (6–8). Diffusion tensor imaging (DTI) has identified depression-related white matter (WM) alterations in these same frontolimbic networks (9,10).

While a number of DTI studies have examined WM differences in depression, the reported location, magnitude, and direction of variance has been heterogeneous. Meta-analyses have reported alterations in the right inferior longitudinal fasciculus, the right inferior fronto-occipital fasciculus, and the superior longitudinal fasciculus (10–12). Some individual studies have reported no significant group differences at all (13,14).

Several rotationally invariant scalar metrics may be calculated from the diffusion tensor, with common choices including fractional anisotropy (FA), mean diffusivity (MD), radial diffusivity (RD), and axial diffusivity (AD) (15). These measures have proven useful for differentiating between clinical and neurotypical groups. However, multiple WM characteristics affect

SEE COMMENTARY ON PAGE 856

ISSN: 2451-9022

each DTI metric, making physiological interpretation difficult. Contributing factors include WM maturation, axonal density, diameter, and integrity; membrane permeability; scan signal-to-noise ratio; and geometrical considerations such as crossing fibers (16,17). FA is the most commonly used DTI metric and provides a summary estimate of the degree to which tissue micro- and macro-organization causes diffusion anisotropy. FA is often discussed as a particularly sensitive index of the integrity of WM: higher values are associated with increased integrity. However, some authors urge caution against overinterpretation of anisotropy results (18,19). MD measures the overall diffusion restriction in a voxel, and lower values are taken to denote more highly organized WM. Finally, AD and RD describe the diffusion magnitude parallel to and perpendicular to the primary diffusion direction, respectively. At least in voxels with a single fiber population, increased RD is associated with demyelination or dysmyelination (20–22), while decreased AD has reflected axonal degeneration or damage (23,24). Thus, in the present study, by examining FA and MD conjointly with RD and AD, it is possible to derive a more comprehensive picture of the neurobiological changes in MDD.

WM FA differences in tracts connecting to the amygdala and hippocampus have been shown to predict remission following antidepressant treatment (25). Long-term normalization of limbic WM FA values following remission has also been observed (26). Further work has examined limbic WM associations with pharmacological treatment response and remission (27,28). These studies showed that nonremission was predicted by a high ratio of FA values in the cingulate portion of the cingulum bundle (CgC) and the stria terminalis. While this work represents progress in the identification of imaging biomarkers of treatment response, it focused only on corticolimbic regions and identified just 29% of nonremitters, albeit with high specificity. Furthermore, almost all studies to date have focused on FA as the primary outcome variable.

The present study is part of the Canadian Biomarker Integration Network in Depression-1 (CAN-BIND-1) study, which examined an MDD population before and during antidepressant treatment using neuroimaging, electroencephalographic, clinical, and molecular measures (29,30). The relatively large sample size allowed an examination of all 4 scalar DTI metrics in WM regions throughout the brain. Broadly, we hypothesized that DTI measures reflect WM changes linked to MDD treatment response in association tracts including the inferior and superior longitudinal fasciculus, uncinate fasciculus, and inferior fronto-occipital fasciculus. Our primary objective was to investigate baseline WM differences associated with response or nonresponse to SSRI treatment in patients with depression. Second, we investigated temporal changes in DTI metrics associated with a favorable medication response during the 8-week study period.

METHODS AND MATERIALS

As part of the CAN-BIND-1 study, participants with a diagnosis of MDD and healthy participants were recruited at 6 sites [for a full description of the clinical and imaging protocols, see Lam *et al.* (29) and MacQueen *et al.* (30)]. Institutional ethics boards at each site gave research ethics approval. All participants gave written informed consent and were compensated for study participation. Sites and participant numbers are shown in Table 1. Individuals with MDD were between 18 and 60 years of age, met DSM-IV-TR (31) criteria for a major depressive episode as identified through the Mini-International Neuropsychiatric Interview (32), had a depressive episode duration of 3 months or longer, were free of psychotropic medication for at least 5 medication half-lives before baseline testing, scored 24 or greater on the Montgomery–Åsberg Depression Rating Scale (MADRS) (33), and had adequate English language fluency for questionnaires and interviews. Exclusion criteria for MDD participants were accompanying psychosis, high risk for hypomanic switch, past failure of 4 or more pharmacological interventions, previous intolerance or nonresponse to escitalopram or aripiprazole, ongoing psychological treatment initiated within the past 3 months, diagnosis of bipolar disorder I/II or other primary psychiatric diagnoses, significant personality disorder that would preclude protocol completion, or high suicide risk. Patients meeting clinical criteria for generalized anxiety disorder were not excluded. Exclusion criteria for control subjects and MDD participants included substance abuse/dependence in past 6 months, significant head trauma/neurological disorders or other unstable medical conditions, pregnancy or breastfeeding, or magnetic resonance imaging contraindications. Images were collected at 3 time points: at baseline, 2 weeks, and 8 weeks following the initiation of a standardized, open-label monotherapy treatment with the SSRI escitalopram (10–20 mg). Preexisting, stable, low doses of zopiclone or lorazepam were allowed to continue. A therapeutic response was established as a 50% reduction in MADRS score between baseline and week 8, dividing the MDD group into responders and nonresponders.

Diffusion images were acquired using a single-shot spin echo echo-planar imaging sequence. Diffusion sensitizing gradients (b = 1000 s/mm^2) were applied along 31 noncolinear directions at most sites, with 30 directions used at sites 3 and

Table 1. Scanning at the 6 Study Sites

Site	Scanner	B_0	MDD Participants, *n* (Female)	Control Subjects, *n* (Female)
1	GE Discovery MR 750	3T	5 (5)	5 (2)
2	GE Discovery MR 750	3T	31 (22)	19 (12)
3	Siemens Tim Trio	3T	20 (9)	16 (12)
4	GE Signa HDxt	3T	55 (34)	25 (16)
5	Philips Achieva	3T	58 (39)	12 (8)
6	GE Discovery MR 750	3T	31 (18)	35 (21)
	Total		200 (127)	112 (71)

All sites used a multichannel receiver head coil. Site locations were 1) the Center for Addiction and Mental Health, Toronto, Ontario, Canada; 2) St Joseph's Healthcare, Hamilton, Ontario, Canada; 3) Queen's University, Kingston, Ontario, Canada; 4) Toronto Western Hospital, Toronto, Ontario, Canada; 5) University of British Columbia, Vancouver, British Columbia, Canada; and 6) University of Calgary, Calgary, Alberta, Canada.

GE Healthcare, Milwaukee, WI; Philips Medical Systems, Best, the Netherlands; Siemens Healthcare GmbH, Erlangen, Germany.

B_0, magnetic resonance imaging background field strength; MDD, major depressive disorder.

5 owing to scanner limitations. Six images without diffusion weighting (b = 0) were also acquired and reconstructed as separate individual images for later processing. Isotropic 2.5-mm voxels were acquired (field of view = 240 × 240 mm, matrix = 96 × 96, 2.5-mm-thick slices, no gap). Depending on the scanner, 52 to 58 axial slices were acquired at each site. The repetition time was 8 seconds and the echo time was 94 ms. One signal average was acquired, with parallel imaging (acceleration factor R = 2). Most sites used image space reconstruction (i.e., GE ASSET and Philips SENSE), while site 3 used the GRAPPA k-space method. The total acquisition took about 5 minutes. Several sites required an adjustment of scan parameters to obtain consensus values after data acquisition had begun. This led to the division of the data into 11 subprojects to account for cross-site differences in later processing (see Supplement).

Image Processing

All diffusion-weighted and T2-weighted (b = 0) images from each participant visit (hereafter, a trial) were combined into a single 4-dimensional NIfTI file. Motion and eddy current correction were applied for each trial using affine registration (eddy_correct), and diffusion vectors rotated accordingly. Background masking was applied. The diffusion tensor model was fit using a weighted-least-squares approach, and FA, MD, RD, and AD scalar maps were calculated in the participant's native space. Spatial normalization was accomplished by nonlinear registration of each trial's FA map to a 2-mm isotropic FA reference in Montreal Neurological Institute (MNI 152) standard space. The FA reference and later discussed regions of interest (ROIs) originated from the Johns Hopkins University ICBM-DTI-81 WM atlas (34), as distributed with FSL version 5.0.10 (http://fsl.fmrib.ox.ac.uk/fsl). To reduce the effects of registration errors and individual variation, the skeletonization step of the tract-based spatial statistics pipeline was applied to the mean FA image (35). For each scalar metric, values from 40 ROIs (listed in the Supplement) were extracted from the projected skeleton of each participant [similar to (36–38)]. In addition, 2 ROIs were generated from the lateralized skeleton periphery outside the Johns Hopkins University regions. These steps were performed using custom-written shell scripts based on FSL tools (39).

Quality control was maintained by examination of color FA glyph images for each participant's baseline scan. This provided visual confirmation that gradient direction definitions and magnitudes had been properly interpreted to generate tensor models. An edge-overlay image of the brain mask on the mean b = 0 image was also examined for every trial, to verify the mask and exclude scans with excessive distortion or signal dropout.

Statistical Methods

To reduce intersite variance, a global scaling method was employed (40). First, using the control subjects within each site, age and sex were regressed from the average of each scalar map (37). Next, ROI residuals were fitted with a linear model to obtain intercepts and slopes representing the site effects for each scalar metric (Supplemental Figure S3). This method and subsequent statistical tests were carried out using custom-written python scripts (39). Analysis proceeded with the residuals of the site-effect regressions after controlling for age and sex.

Intrasubject data reliability was assessed using the sum of squared errors (SSE) from linear fits to the 3 data points of each participant for each ROI and DTI metric. Outliers were identified based on extreme SSE values compared with their study group ($z > 2.67$, at least). Next, to ensure that results were not biased by extreme values, data points were identified for imputation based on comparison with their group distribution (distribution-based outlier [DIST] strategy) ($z > 3.02$, at least). Based on the SSE and DIST strategies, 4 outlier approaches were enacted: EX0, in which no outliers were imputed; EX1, using the SSE strategy only; EX2, using both SSE and DIST strategies; and EX3, in which the SSE strategy was extended so that participants with high mean SSE had all their values imputed, and the DIST strategy was run twice.

Group differences between MDD participants and control subjects in baseline scans were assessed for each ROI using 2-sample t tests, followed by a false discovery rate procedure to control for multiple comparisons (41). A 3-way analysis of variance was used to test for responder, nonresponder, and control group effects in baseline scans, followed by a post hoc Tukey honestly significant difference test for pairwise differences. Because not all participants remained in the study at week 8, baseline comparisons included more participants than statistical tests involving all 3 time points (see Table 2).

Table 2. Participant Demographics and Symptom Severity

Group	Baseline[a], n	3 Visits[b], n	Age, Years, Mean ± SD	Sex Ratio (Female/Male)	MADRS Score, Mean ± SD	Motion, mm, Mean ± SD	Outlier Strategy[c]	
							SSE	DIST
Control	103	86	33.2 ± 10.7	1.77	0.8 ± 1.6	0.71 ± 0.67	1.2	2.4
Responder	80	66	34.6 ± 11.7	1.75	29.8 ± 5.4	0.79 ± 0.80	0.9	4.3
Nonresponder	85	71	36.8 ± 13.4	1.63	30.7 ± 5.4	0.74 ± 0.49	0.8	1.7

Of the 312 participants listed in Table 1, 308 had scans at baseline, and a further 17 baseline scans were excluded in quality control. This left 291 participants: 103 control subjects and 188 MDD participants, which were used in the baseline t tests. As the designation of responders and nonresponders occurred at week 8, and some participants did not attain week 8 in the study, only 80 + 85 = 165 major depressive disorder participants were used in the 3-group analysis of variance at baseline. Motion measures indicate average displacement.

DIST, distribution-based outlier; MADRS, Montgomery–Åsberg Depression Rating Scale; SSE, sum of squared errors.

[a]Participants included in statistical analyses at baseline.

[b]Participants with valid scans from all 3 visits, which were included in the mixed-effects regression analyses.

[c]Outlier counts represent the mean number of values imputed across regions of interest for the fractional anisotropy metric.

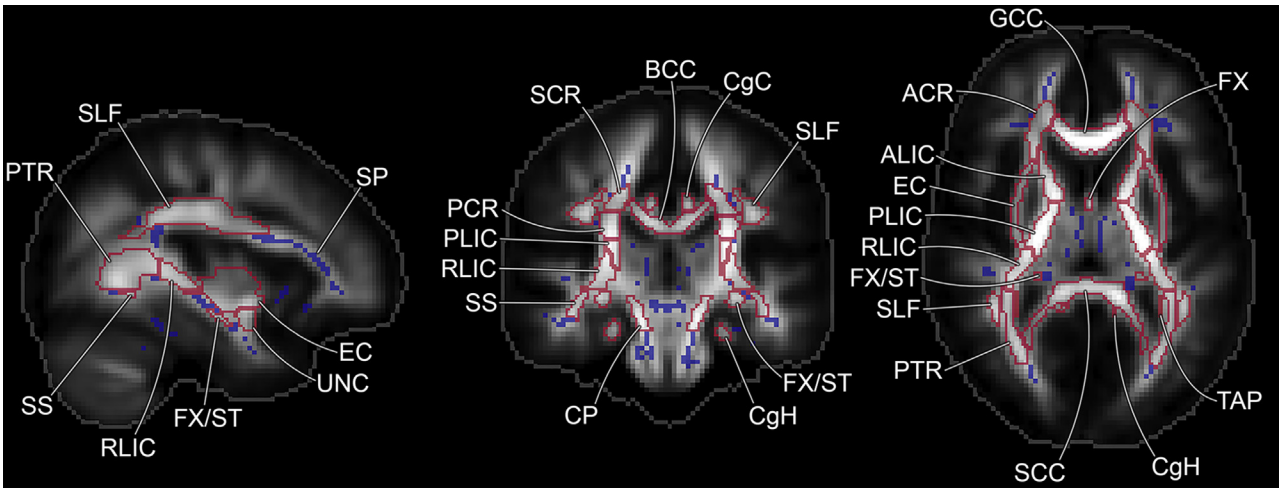

Figure 1. Regions of interest (in red) and peripheral skeleton (SP) (in blue) overlaid on the mean fractional anisotropy image from the Johns Hopkins University ICBM-81 atlas. The gray outline represents the brain mask boundary. Left/right region-of-interest labels have been omitted for brevity. The views are centered on (−34 mm, −24 mm, 8 mm) in Montreal Neurological Institute (MNI) coordinates to show the regions with significant results in this study, and are shown in radiological orientation. The maximum grayscale value of the underlay was set to fractional anisotropy = 0.6. A full region-of-interest list is in the Supplement. Those shown here are the anterior corona radiata (ACR), anterior limb of internal capsule (ALIC), body of corpus callosum (BCC), cingulum (cingulate gyrus) (CgC), cingulum (hippocampus) (CgH), cerebral peduncle (CP), external capsule (EC), fornix (column and body of fornix) (FX), fornix (cres)/stria terminalis (FX/ST), genu of corpus callosum (GCC), posterior corona radiata (PCR), posterior limb of internal capsule (PLIC), posterior thalamic radiation (PTR), retrolenticular part of internal capsule (RLIC), splenium of corpus callosum (SCC), superior corona radiata (SCR), superior longitudinal fasciculus (SLF), sagittal stratum (SS), tapetum (TAP), and uncinate fasciculus (UNC).

To assess temporal changes in DTI metrics and fully leverage the longitudinal character of the data set, linear mixed-effects regression (LMER) was employed (42,43). Time and group were considered fixed effects in the model, while individual participants were considered random. The maximum likelihood ratio test was used to evaluate significance. More details on LMER and the following outlier strategies are given in the Supplement.

To assess test–retest reliability, intraclass correlation coefficient (ICC) values were calculated before outlier detection. The form was *ICC*(3,1) as defined by Shrout and Fleiss (44), because of the fixed time points used in this study. Effect sizes (*d*) on group differences were calculated as mean differences normalized by pooled standard deviations (45).

RESULTS

Figure 1 shows highly pertinent ROIs overlaid on the mean FA image. The full extent of some regions can be difficult to visualize from plane views. In particular, it is noteworthy that the CgC and cingulum hippocampus (CgH) ROIs curve around and meet posterior to the corpus callosum. The volumes of all ROIs examined are detailed in the Supplement. The fornix ROI was excluded from analysis as it was found to be severely corrupted by partial volume of cerebrospinal fluid: median MD in the fornix was 1.31 compared with a range of 0.64 to 0.81 in all other ROIs.

During quality control, 25 scans were excluded (17 baseline; 20 participants represented), mainly owing to artifacts of distortion or signal, which were identified when checking the mask images. Viewing all participant visits sequentially was particularly effective for identifying abnormal distortion. Several irregularities were also identified from the glyph images. There were no group differences in average displacement calculated from motion-correction parameters ($F_{2,666} = 0.969$, $p = .394$ by permutation test). The final participant group numbers, demographics, and symptom severity scores are listed in Table 2. Group differences in age ($F_{2,220} = 1.728$, $p = .18$), sex ($F_{2,220} = 0.036$, $p = .96$), and baseline MADRS depression scores between responders and nonresponders ($F_{1,135} = 0.828$, $p = .36$) were not significant.

The global scaling method decreased intersite variance (Supplemental Figure S1), as demonstrated by the decreased spread of the colored site-mean lines. Quantitatively, after applying global scaling (but without outlier imputation), the standard deviation of the site means for each metric decreased by 34% to 49%.

The mean ICC values of control subjects in the global scaled data, before outlier imputation, were 0.82 (FA), 0.75 (MD), 0.75 (AD), and 0.80 (RD). Values were slightly higher before global scaling, by 0.05 on average. This can be interpreted based on the changes in session and participant variances: intersession variance decreased by only 3% with global scaling, while intersubject variance decreased by 24%. So, decreased intersite variance led to the decrease in ICC. ICC was not strongly correlated with DTI metric values across ROIs ($|r| < .25$ in all 4 cases).

The outlier identification approaches affected the LMER results in a limited way. With no imputation at all, the EX0 approach returned 59 significant group differences, while 55, 64, and 71 significant results came from the EX1, EX2, and EX3 approaches, respectively. The effect sizes increased when DIST strategy outliers were excluded, with mean effect sizes of 0.49, 0.49, 0.51, and 0.53 from the 4 approaches (EX0, EX1, EX2, and EX3, respectively). To balance the desire to keep as much data as possible, while still ensuring that results were not biased by low-quality or extreme values, the subsequently reported LMER results used the EX2 approach.

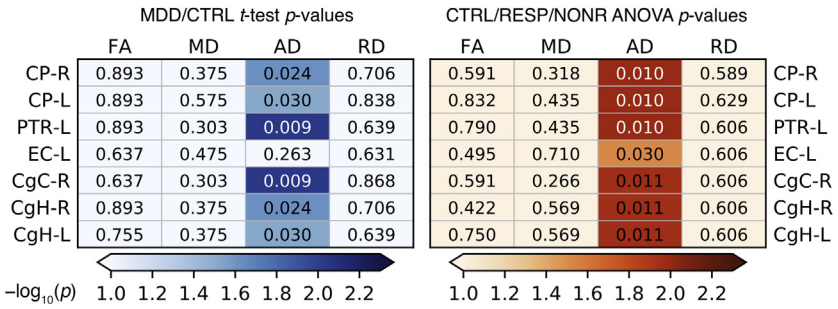

Figure 2. Regions with significant effects in the baseline data. Values shown within the grids are false discovery rate–corrected p values, while the colors are mapped to $-\log_{10}(p)$, so that darker indicates greater significance. (Left) False discovery rate–corrected p values from the major depressive disorder (MDD) and control (CTRL) group t tests. Only the axial diffusivity (AD) metric indicated significant group differences after multiple comparison correction. (Right) False discovery rate–corrected p values from the CTRL/responder (RESP)/nonresponder (NONR) analysis of variance (ANOVA). In post hoc tests, the only region with a significant responder/nonresponder difference was the left external capsule (EC-L). CgC-R, right cingulum cingulate; CgH-L, left cingulum hippocampus; CgH-R, right cingulum hippocampus; CP-L, left cerebral peduncle; CP-R, right cerebral peduncle; FA, fractional anisotropy; MD, mean diffusivity; PTR-L, left posterior corona radiata; RD, radial diffusivity.

Baseline Scans

Testing for ROI-based group differences in baseline scans identified very few significant results that survived multiple-comparison correction. The EX0 and EX1 approaches revealed no significant effects, whether testing MDD participants against control subjects, or among responders, nonresponders, and control subjects. Group differences were found using EX2, all confined to the AD metric (Figure 2). Compared with the control group, reduced AD was found in the MDD group with false discovery rate–corrected $p < .05$ in 6 regions: right cerebral peduncle (CP-R), left cerebral peduncle (CP-L), left posterior thalamic radiation (PTR-L), right CgC (CgC-R), right CgH (CgH-R), and left CgH (CgH-L).

The 3-way analysis of variance dividing responders from nonresponders indicated AD group differences in the same 6 regions, as well as left external capsule (EC-L). Pairwise post hoc tests showed decreased AD in nonresponders compared with control subjects in the CP-R, CP-L, PTR-L, CgH-R, and CgH-L. Responders had decreased AD compared with control subjects in the PTR-L and CgC-R, but elevated AD compared with control subjects and nonresponders in the EC-L. Baseline testing results from the EX3 approach were almost identical to EX2, with the addition of decreased AD in nonresponders compared with control subjects in the right sagittal stratum (SS-R) region.

Regression Analysis

Using the LMER method and the maximum likelihood ratio test significance test with the EX2 outlier approach yielded significant baseline group effects in 15 regions for FA, 8 for MD, 20 for AD, and 6 for RD (Figure 3). The significant group differences

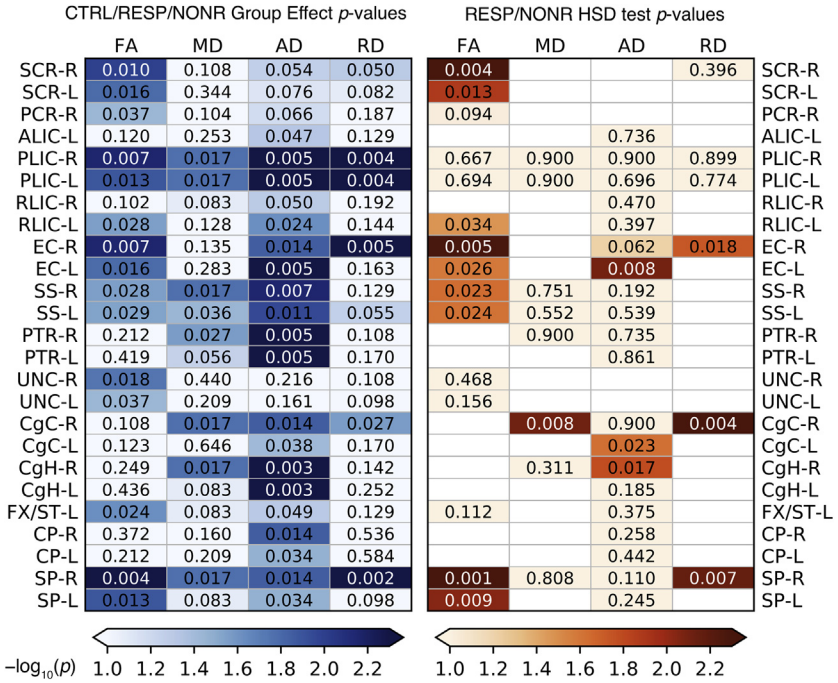

Figure 3. Regions with significant baseline effects from the linear mixed-effects regression analysis. As in Figure 2, colors represent $-\log_{10}(p)$ of the p values shown within the grids. (Left) False discovery rate–corrected p values for group effects from the maximum likelihood ratio test. It is noteworthy that using fractional anisotropy (FA) as the sole outcome metric would have missed several strong group effects, particularly in the posterior thalamic radiation (PTR) and cingulum regions (cingulum cingulate [CgC], cingulum hippocampus [CgH]). (Right) Corrected p values for responder (RESP)/nonresponder (NONR) difference from the Tukey honestly significant difference (HSD) test. Blank cells occur because only regions with a significant trigroup effect were tested post hoc. The superior corona radiata (SCR), external capsule (EC), sagittal stratum (SS), and both cingulum regions (CgC, CgH) strongly differentiated medication RESPs from NONRs. AD, axial diffusivity; ALIC, anterior limb of internal capsule; CP, cerebral peduncle; CTRL, control; FX/ST, fornix (cres)/stria terminalis; L, left; MD, mean diffusivity; PCR, posterior corona radiata; PLIC, posterior limb of internal capsule; R, right; RD, radial diffusivity; RLIC, retrolenticular part of internal capsule; SP, peripheral skeleton; UNC, uncinate fasciculus.

ROI	Groups	Metric	Direction	Δ	d	Sig
CP-R	N – C	AD	N ▼	-0.035	-0.47	
CP-L	N – C	AD	N ▼	-0.031	-0.41	
PLIC-R	N – C	FA	N ▲	0.013	0.43	
"	"	AD	N ▼	-0.028	-0.52	**
"	"	MD	N ▼	-0.014	-0.53	
"	"	RD	N ▼	-0.018	-0.53	**
"	R – C	FA	R ▲	0.018	0.54	**
"	"	AD	R ▼	-0.027	-0.53	**
"	"	MD	R ▼	-0.014	-0.52	
"	"	RD	R ▼	-0.020	-0.57	**
PLIC-L	N – C	AD	N ▼	-0.029	-0.49	
"	"	MD	N ▼	-0.015	-0.48	
"	"	RD	N ▼	-0.020	-0.49	**
"	R – C	FA	R ▲	0.020	0.54	
"	"	AD	R ▼	-0.037	-0.68	**
"	"	MD	R ▼	-0.016	-0.52	
"	"	RD	R ▼	-0.025	-0.62	**
RLIC-L	N – C	AD	N ▼	-0.018	-0.42	
"	N – R	FA	R ▲/N ▼	-0.010	-0.43	
SCR-R	N – R	FA	R ▲/N ▼	-0.012	-0.54	**
"	R – C	RD	R ▼	-0.009	-0.42	
SCR-L	N – R	FA	R ▲/N ▼	-0.012	-0.49	
"	R – C	FA	R ▲	0.011	0.44	
PTR-R	N – C	AD	N ▼	-0.032	-0.52	**
"	"	MD	N ▼	-0.015	-0.38	
"	R – C	AD	R ▼	-0.024	-0.40	
PTR-L	N – C	AD	N ▼	-0.035	-0.49	
"	R – C	AD	R ▼	-0.029	-0.44	
SS-R	N – C	AD	N ▼	-0.022	-0.54	
"	"	MD	N ▼	-0.010	-0.37	
"	N – R	FA	R ▲/N ▼	-0.014	-0.43	
"	R – C	MD	R ▼	-0.013	-0.49	
SS-L	N – C	AD	N ▼	-0.024	-0.60	**
"	N – R	FA	R ▲/N ▼	-0.011	-0.43	
"	R – C	MD	R ▼	-0.015	-0.59	**
EC-R	N – C	FA	N ▼	-0.013	-0.51	**
"	"	RD	N ▲	0.017	0.55	**
"	N – R	FA	R ▲/N ▼	-0.014	-0.52	**
"	"	RD	N ▲	0.014	0.44	
"	R – C	AD	R ▲	0.014	0.48	
EC-L	N – C	FA	N ▼	-0.012	-0.43	
"	N – R	FA	R ▲/N ▼	-0.012	-0.43	
"	"	AD	R ▲	-0.021	-0.50	**
"	R – C	AD	R ▲	0.022	0.58	**
CgC-R	N – C	AD	N ▼	-0.024	-0.49	
"	N – R	MD	R ▼	0.014	0.51	
"	"	RD	N ▲/R ▼	0.019	0.53	
"	R – C	AD	R ▼	-0.022	-0.41	
"	"	MD	R ▼	-0.016	-0.64	
CgC-L	N – R	AD	R ▲/N ▼	-0.030	-0.45	
CgH-R	N – C	AD	N ▼	-0.057	-0.76	***
"	"	MD	N ▼	-0.023	-0.55	
"	N – R	AD	N ▼	-0.034	-0.46	
CgH-L	N – C	AD	N ▼	-0.069	-0.76	***
"	R – C	AD	R ▼	-0.042	-0.55	
UNC-R	N – C	FA	N ▼	-0.020	-0.48	
SP-R	N – C	AD	N ▼	-0.012	-0.49	
"	N – R	FA	R ▲/N ▼	-0.009	-0.59	**
"	"	RD	R ▼	0.010	0.52	**
"	R – C	FA	R ▲	0.007	0.49	**
"	"	MD	R ▼	-0.008	-0.44	
"	"	RD	R ▼	-0.012	-0.69	***
SP-L	N – C	AD	N ▼	-0.010	-0.41	
"	N – R	FA	R ▲/N ▼	-0.008	-0.52	

Figure 4. Significant group differences detected by the linear mixed-effects regression approach. These regions had significant group effects (false discovery rate–corrected $p < .05$) from the likelihood ratio test, and showed significant group differences in post hoc Tukey honestly significant difference (HSD) tests with $\alpha = .05$. Group differences at false discovery rate–corrected $^{**}p < .01$ and $^{***}p < .001$. Ditto marks (") indicate an identical value to above, and fractional anisotropy (FA) and mean diffusivity (MD) results have been highlighted in green. Particularly strong effect sizes were found in the nonresponder (N)/control (C) group difference in the cingulum hippocampus region and the sagittal stratum. The highest effect sizes for the responder (R)/control comparison were found in the internal capsule (posterior limb of internal capsule [PLIC]) and cingulum (cingulate gyrus) (CgC) regions. Δ, difference of group means; AD, axial diffusivity; CgH, cingulum hippocampus; CP, cerebral peduncle; *d*, effect size; EC, external capsule; L, left; PTR, posterior thalamic radiation; R, right; RD, radial diffusivity; ROI, region of interest; SCR, superior corona radiata; SP, peripheral skeleton; SS, sagittal stratum; UNC, uncinate fasciculus.

from post hoc tests are reported in Figure 4, while Figures 5 and 6 show additional plots of key group differences.

No significant temporal trends in any group's DTI metrics were observed over the 8-week observation period of this study. No groups had significantly nonzero slope values, and none had group differences in slope. Taking the responders group as a typical example, the mean slope in FA across ROIs was −0.00004, compared with a mean intercept of 0.63, and the average ratio of the SE to the magnitude of the slope was 4.0.

DISCUSSION

In the present study we examined whether a positive therapeutic response to SSRIs in depressed patients was associated with WM microstructural differences, as measured by DTI. Imaging data were collected at 3 time points in patients and control subjects, and a therapeutic response to SSRI was established by a 50% reduction of depressive symptoms as assessed by MADRS at 8 weeks.

Our findings present the general pattern that nonresponder/control group differences had greater magnitude than responder/control group differences. Furthermore, the results pointed to decreased WM integrity in nonresponders. Noting that decreased AD, increased RD, and decreased FA are generally taken to indicate WM disruption (20–24), every ROI with significant group effects in the LMER analysis indicated reduced integrity of WM in nonresponders.

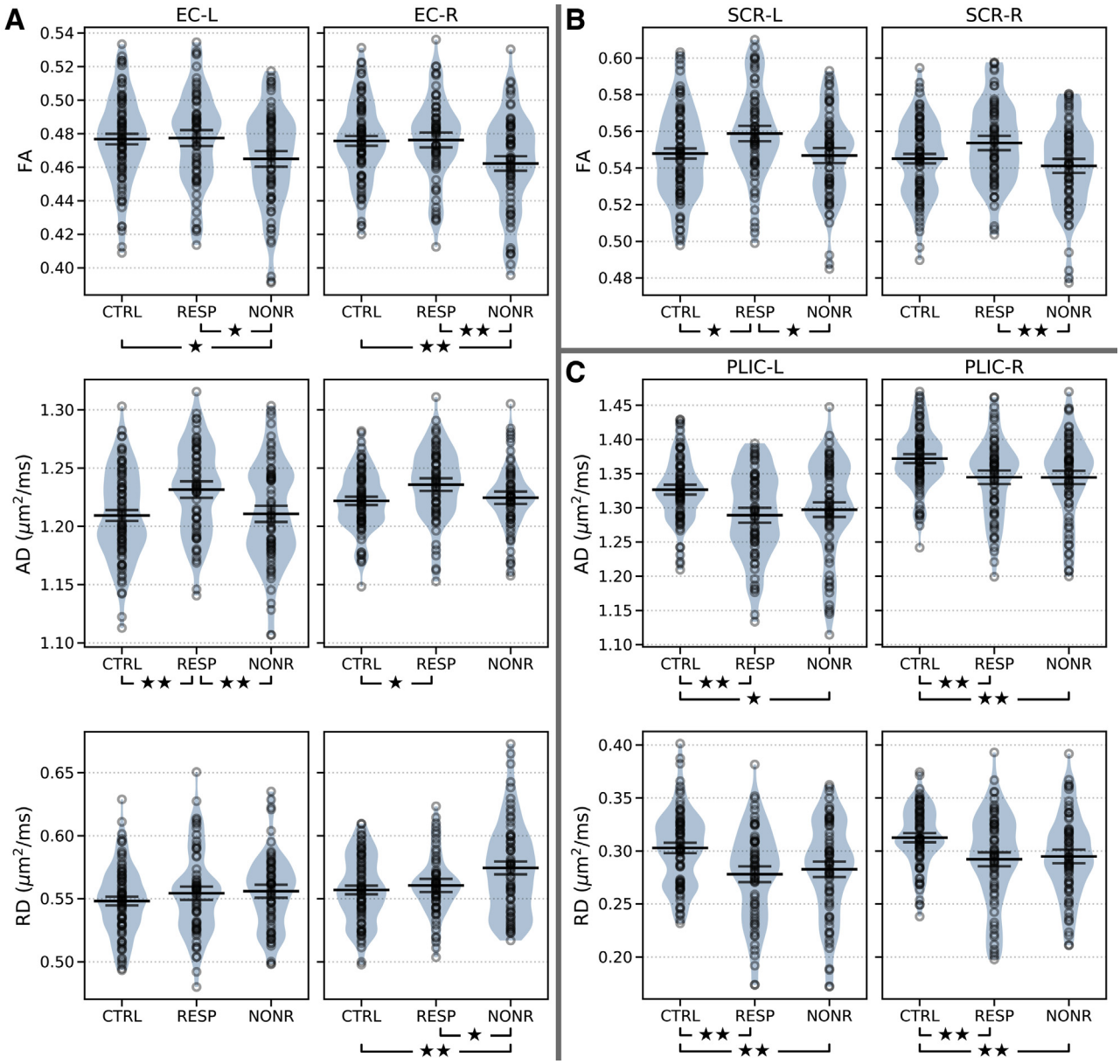

Figure 5. Group comparisons for selected cortical connecting tracts. The plot symbols represent baseline values from the linear mixed-effects regression intercepts. Shaded regions show the data distribution with kernel density estimation (violin plot) (72). Horizontal lines represent group means with standard errors from the model fits. The level of significant group difference is indicated as ★ ($p < .05$), ★★ ($p < .01$), or ★★★ ($p < .001$). **(A)** Three metrics in the external capsule (EC), a region that overlaps the superior longitudinal fasciculus; all 3 study groups are strongly discriminated when including all the metrics, and it can be seen that radial diffusivity (RD) is driving the fractional anisotropy (FA) changes more than axial diffusivity (AD). **(B)** FA in the superior corona radiata (SCR); the groups are differentiated mainly due to elevated FA in responders. **(C)** AD and RD values in the posterior limb of internal capsule (PLIC) region; the relative differences in group means show remarkable bilateral symmetry, with both responders (RESPs) and nonresponders (NONRs) differentiated from control (CTRL) subjects by decreased AD and RD. L, left; R, right.

Group differences identified from the baseline scans were limited to the AD measure (Figure 2). Alterations were identified in a number of regions previously associated with WM changes in depression: the EC-L, PTR-L, the cingulum (cingulate gyrus [CgC-R]), and bilateral CP and cingulum (hippocampus [CgH]). These group differences in AD may reflect WM disruption in MDD, as reduced AD has been associated with axonal degeneration in mouse models (23). This is consistent with prior work that has shown spectroscopic indicators of aberrant cell membrane turnover and changes in neuronal/axonal integrity (46) in chronic depression (47–49). The limited group differences in baseline DTI scans, confined only to AD, were in line with some previous literature that has not found MDD/control group differences when only testing FA (14). The regression (LMER) analysis was employed to leverage the full temporal nature of this study (i.e., baseline,

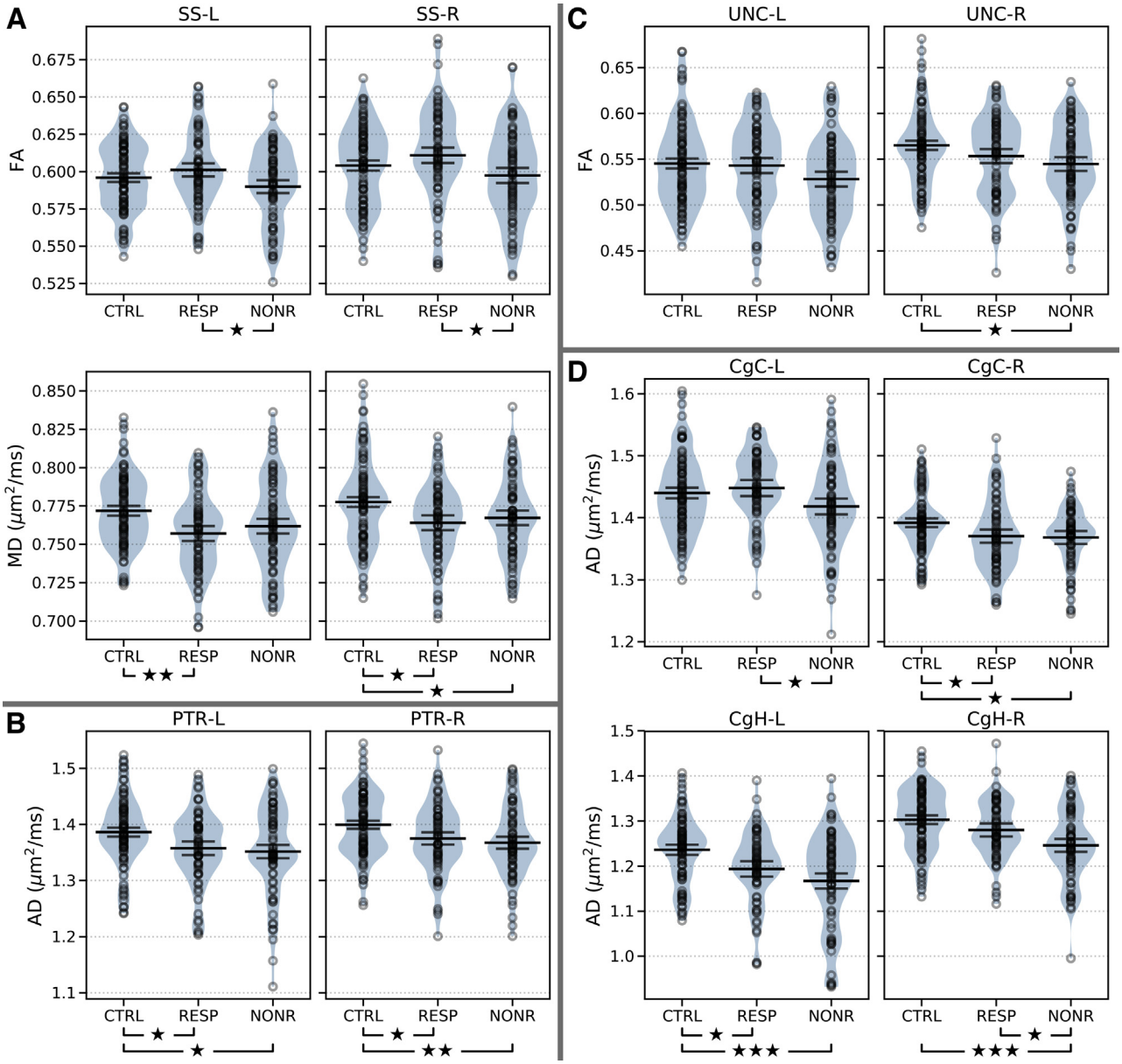

Figure 6. Group comparisons in frontotemporal white matter tracts. The level of significant group difference is indicated as ★ ($p < .05$), ★★ ($p < .01$), or ★★★ ($p < .001$). **(A)** Baseline (linear mixed-effects regression intercept) values from the sagittal stratum (SS) regions. Highly symmetrical trends show elevated fractional anisotropy (FA) in responders (RESPs) that differentiated them from nonresponders (NONRs), while mean diffusivity (MD) was decreased compared with control (CTRL) subjects in both major depressive disorder groups. **(B)** In the posterior thalamic radiation (PTR), decreased axial diffusivity (AD) values distinguished both major depressive disorder groups from CTRL subjects. **(C)** In the uncinate fasciculus (UNC), symmetrical trends in group mean values significantly differentiated NONRs from CTRL subjects. **(D)** In the cingulum regions (cingulum cingulate gyrus [CgC]), especially the cingulum hippocampus (CgH), decreased AD distinguished NONRs from CTRL subjects. RESPs generally fell in between, and were distinguished from the other 2 groups in several regions. The effect size of the NONR/CTRL difference in the left CgH (CgH-L) was the strongest in this study ($d = -0.76$). The trends in responder AD values in the CgC regions were a rare example of bilateral asymmetry. L, left; R, right.

week 2, and week 8). We found that none of the groups had significantly nonzero regression slopes, and there were no group differences in regression slopes in any metric (FA, MD, AD, RD). Therefore, there were no apparent SSRI-propagated WM changes across the 8-week time span of this study.

However, the LMER intercept values identified baseline group differences that encompassed the baseline-scan AD results, and also identified several effects in RD, FA, and MD (Figure 3). Additional WM alterations were identified in the superior corona radiata (SCR), internal capsule (especially the posterior limb of the internal capsule), SS, and uncinate fasciculus (UNC). We suggest that LMER had greater sensitivity at baseline owing to the reduction in random variance that resulted from using all 3 time points. These observations are

consistent with neuroimaging work illustrating that multiple acquisitions from individual participants elucidate finer regional features and improve the resolution of network characteristics [e.g., (50)]. In interpreting our results, FA and MD may be regarded as derived metrics. They are useful for comparison to prior literature, as they have been widely used. AD and RD provide valuable clarification of the observed effects, as basic studies have tied these metrics directly to WM disruption with an identifiable cause.

Cortical Systems: Corona Radiata, Internal Capsule, and EC

Higher FA distinguished responders from both control subjects and nonresponders in the SCR. The SCR is an area of interdigitated WM that comprises a mixed fiber population, notably including projections that traverse the internal capsule and radiate to the cortices (51), and corticostriatal fibers (52,53). Prior studies have reported altered MD in the SCR of depressed participants (54). WM differences found here in the SCR and posterior limb of the internal capsule of responders may reflect network connectivity changes that are associated with the psychomotor disturbances in MDD (55,56).

Several WM changes were observed in the EC ROI, considered part of the superior longitudinal fasciculus, which were similar to previous reports from melancholic MDD (57) and treatment-resistant MDD (58). Importantly, nonresponders were differentiated from responders bilaterally in FA, driven by changes in both RD and AD. The EC carries fibers directly from the prefrontal cortex to the striatum (59) and has been associated with social reward processing (60). As such, these findings are in line with research that has emphasized disrupted reward circuitry in depression (12,61).

Frontotemporal WM: SS, UNC, and the Cingulum

Several DTI metrics in the SS distinguished the 3 groups, with nonresponders consistently having lower FA and AD values. The SS includes association fibers of the inferior longitudinal fasciculus and inferior fronto-occipital fasciculus. A meta-analysis (10) found lower FA in the right inferior longitudinal fasciculus and right inferior fronto-occipital fasciculus in MDD, and decreased FA in SS in MDD is consistent with prior literature (62).

We also found that reduced FA in the right UNC distinguished nonresponders from control subjects (Figure 5). The UNC connects the orbital and medial prefrontal cortices and the anterior mesial temporal lobe (63–65) and is functionally important in the regulation of social and emotional behavior (66–68).

Our findings particularly highlight the cingulum areas to distinguish responders from nonresponders. The AD metric most reliably differentiated the groups, with nonresponders consistently having the lowest values. The cingulum bundle lies deep to the cortical gray matter of the cingulate gyrus, extending from Brodmann area 25 to the amygdala and hippocampus (69). In the ICBM-DTI-81 atlas, the cingulum is divided at the level of the splenium of the corpus callosum into the CgH inferiorly and the CgC superiorly. The related literature includes reports of WM FA reductions in the cingulum (12,68,70), reports that CgC FA was predictive of medication response (27), and functional magnetic resonance imaging research identifying the subgenual anterior cingulate as a locus of treatment response (71).

Taken together, the results from the SS, UNC, and cingulum may suggest that a positive therapeutic response to SSRIs is contingent on intact corticolimbic connectivity. These findings also complement evidence that participants with treatment-resistant MDD show greater reductions in FA in WM regions including UNC and CgC, as compared with first-episode participants and control subjects (58).

Limitations and Implications for Future Studies

One limitation of this study concerns the relatively short study duration. It is possible that plasticity in the WM alterations of responders would have become apparent on a longer time scale, such as a 6-month follow-up (26). The exclusion of the fornix, a tract of particular interest in MDD (27), was a further limitation. However, diffusivity values indicated that it was heavily corrupted by partial volume of cerebrospinal fluid. Fitting an advanced diffusion model that includes a cerebrospinal fluid compartment may remedy this limitation.

In this study, intersubject variance was clearly increased by the use of multiple study sites, and in particular, scanner manufacturers (Supplemental Figure S3). Although the linear regression method used here greatly reduced the variance (Supplemental Figure S1), some nonlinear effects may have remained as a confound.

It was evident from the 4 outlier identification approaches that more aggressive outlier cleaning methods produced more results from significance tests. This indicates that extreme values were inflating variance in the dataset, rather than driving the significance of results, and lends credence to the effects identified here. In addition, incorporating 3 measurements into the analysis reduced intrasubject variance and identified more group differences. This further points to random variance as a significant impediment to revealing differences between groups in DTI studies of MDD. Future studies would likely benefit from acquiring the equivalent of all 3 scans in this study during the baseline visit alone (e.g., 1 high angular resolution diffusion imaging scan). The examination of all 4 scalar DTI metrics was also beneficial and should be adopted in future research.

Conclusions

Baseline DTI scans of AD, a metric sometimes associated with axonal integrity, have been shown to distinguish future SSRI responders, nonresponders, and control subjects in several regions. Moreover, we have demonstrated that some of these regions, which have previously been associated with altered WM in MDD, could serve as markers of medication response. Only the EC, a portion of the superior longitudinal fasciculus, was observed to distinguish nonresponders from responders in scans acquired at baseline. However, further baseline responder/nonresponder differences were revealed when all 3 measurements were incorporated in the mixed-effects regression analysis. These findings demonstrate that baseline DTI measures are associated with medication response in MDD, and consideration must be given to intrasubject

variability and outlier classification. Especially strong effects were observed in the cingulum regions and EC, both of which differentiated all 3 groups from one another. We anticipate that future studies will investigate measures from these regions as predictive biomarkers.

ACKNOWLEDGMENTS AND DISCLOSURES

This work was supported by the Ontario Brain Institute, the Canadian Institutes of Health Research, Lundbeck, Bristol-Myers Squibb, and Servier. CAN-BIND is an Integrated Discovery Program carried out in partnership with, and financial support from, the Ontario Brain Institute, an independent nonprofit corporation, funded partially by the Ontario government. The opinions, results, and conclusions are those of the authors and no endorsement by the Ontario Brain Institute is intended or should be inferred. Funding or in-kind support is also provided by the investigators' universities and academic institutions. All study medications are independently purchased at wholesale market values.

Members of the CAN-BIND Investigator Team are listed at www.canbind.ca/our-team.

RWL has received honoraria for ad hoc speaking or advising/consulting, or research funds, from Akili, Allergan, Asia-Pacific Economic Cooperation, BC Leading Edge Foundation, Brain Canada, Canadian Institutes of Health Research, Canadian Network for Mood and Anxiety Treatments, Canadian Psychiatric Association, CME Institute, Hansoh, Janssen, Lundbeck, Lundbeck Institute, Medscape, Mind Mental Health Technologies, Otsuka, Pfizer, St. Jude Medical, University Health Network Foundation, and VGH Foundation. RM is a member of advisory boards and/or speaker's bureaus for the following organizations: Lundbeck, Pfizer, Shire, Sunovion, Janssen, Allergan, BMS, Otsuka; and has received research grants and participated in clinical trials for Lundbeck, Merck, Pfizer, BI, Janssen, CIHR, OBI, CAN-BIND, OMHF; and received presenter honorariums from: Lundbeck, Pfizer, Shire, Sunovion, Allergan, BMS, Otsuka, Janssen. BNF has received consulting fees from Otsuka and a research grant from Pfizer. LM has received grant or research support from the Alternative Funding Plan Innovation Fund, the Brain and Behavioral Foundation, the Canadian Institutes of Health Research, the Hamilton Health Sciences Foundation, the Ontario Brain Institute, and the Ontario Mental Health Foundation; he has served as a consultant or speaker for Bristol-Myers Squibb, the Canadian Psychiatric Association, the Canadian Network for Mood and Anxiety Treatments, and Lundbeck. SCS receives funding from the OBI and CIHR (MOP137097) for neuroimaging analysis in CAN-BIND and he is the Chief Scientific Officer of ADMdx, Inc., a neuroimaging consulting company. GMM has received consulting fees from Pfizer, Lundbeck, Janssen, Johnson & Johnson; honoraria for lectures for Lundbeck and Allergen; and research funding from the OBI and CIHR. SHK is/or has been an advisor/consultant for Abbott, Alkermes, Allergan, BMS, Janssen, Lundbeck, Lundbeck Institute, Otsuka, Pfizer, Servier, Sunovion; participated in clinical trials/studies for Abbott, BMS, Janssen, Pfizer, Servier; performed speaking engagements with the following organizations: BMS, Lundbeck, Pfizer, Servier, Xian-Janssen; and received research support from OBI, CIHR, BMS, Brain Canada, Janssen, Lundbeck, ORF, Pfizer, and Servier. All other authors report no biomedical financial interests or potential conflicts of interest.

ClinicalTrials.gov: Canadian Biomarker Integration Network for Depression Study (CAN-BIND-1); https://clinicaltrials.gov/ct2/show/NCT01655706?term=Integrated+Biological+Markers+for+the+Prediction+of+Treatment+Response+in+Depression&cond=Depression&rank=1; NCT01655706.

ARTICLE INFORMATION

From the Department of Psychology, Neuroscience & Behavior (ADD, GBH) and Department of Psychiatry and Behavioural Neurosciences (BNF, LM), McMaster University, Hamilton; Imaging Research Center (ADD, GBH) and Women's Health Concerns Clinic (BNF, LM), St. Joseph's Healthcare Hamilton, Hamilton; Department of Psychology (RM), Queen's University, and Department of Psychiatry (RM), Queen's University and Providence Care Hospital, Kingston; Rotman Research Institute (SRA, MZ, SCS), Baycrest Centre, Toronto; Department of Psychiatry (SR, SHK), Faculty of Medicine, University of Toronto; Department of Psychiatry (SR, SHK), St. Michael's Hospital; Department of Medical Biophysics (SCS), University of Toronto; Department of Psychiatry (SR, SHK), Krembil Research Centre, University Health Network; and Keenan Research Centre for Biomedical Science (SR, SHK), Li Ka Shing Knowledge Institute, St. Michael's Hospital, Toronto, Ontario; Department of Psychiatry (SH, GMM), Cumming School of Medicine, University of Calgary, Calgary; and Department of Computer Science (JH), University of Alberta, Edmonton, Alberta; and the Department of Psychiatry (RWL), University of British Columbia, Vancouver, British Columbia, Canada.

Address correspondence to Geoffrey B. Hall, Ph.D., Department of Psychology, Neuroscience & Behaviour, McMaster University, 1280 Main Street West, Hamilton, ON L8S 4K1, Canada; E-mail: hallg@mcmaster.ca.

Received Apr 25, 2019; accepted May 28, 2019.

Supplementary material cited in this article is available online at https://doi.org/10.1016/j.bpsc.2019.05.016.

REFERENCES

1. Hansen R, Gaynes B, Thieda P, Gartlehner G, Deveaugh-Geiss A, Krebs E, Lohr K (2008): Meta-analysis of major depressive disorder relapse and recurrence with second-generation antidepressants. Psychiatr Serv 59:1121–1130.
2. Mayberg HS (2003): Positron emission tomography imaging in depression: A neural systems perspective. Neuroimaging Clin N Am 13:805–815.
3. Drevets WC, Price JL, Furey ML (2008): Brain structural and functional abnormalities in mood disorders: Implications for neurocircuitry models of depression. Brain Struct Funct 213:93–118.
4. Koenigs M, Grafman J (2009): The functional neuroanatomy of depression: Distinct roles for ventromedial and dorsolateral prefrontal cortex. Behav Brain Res 201:239–243.
5. Groenewold NA, Opmeer EM, de Jonge P, Aleman A, Costafreda SG (2013): Emotional valence modulates brain functional abnormalities in depression: Evidence from a meta-analysis of fMRI studies. Neurosci Biobehav Rev 37:152–163.
6. Arnone D, McKie S, Elliott R, Thomas EJ, Downey D, Juhasz G, *et al.* (2012): Increased amygdala responses to sad but not fearful faces in major depression: Relation to mood state and pharmacological treatment. Am J Psychiatry 169:841–850.
7. Delaveau P, Jabourian M, Lemogne C, Guionnet S, Bergouignan L, Fossati P (2011): Brain effects of antidepressants in major depression: A meta-analysis of emotional processing studies. J Affect Disord 130:66–74.
8. Gotlib IH, Hamilton JP (2008): Neuroimaging and depression: Current status and unresolved issues. Curr Dir Psychol Sci 17:159–163.
9. Sexton CE, Mackay CE, Ebmeier KP (2009): A systematic review of diffusion tensor imaging studies in affective disorders. Biol Psychiatry 66:814–823.
10. Liao Y, Huang X, Wu Q, Yang C, Kuang W, Du M, *et al.* (2013): Is depression a disconnection syndrome? Meta-analysis of diffusion tensor imaging studies in patients with MDD. J Psychiatry Neurosci 38:49–56.
11. Murphy ML, Frodl T (2011): Meta-analysis of diffusion tensor imaging studies shows altered fractional anisotropy occurring in distinct brain areas in association with depression. Biol Mood Anxiety Disord 1:3.
12. Bracht T, Linden D, Keedwell P (2015): A review of white matter microstructure alterations of pathways of the reward circuit in depression. J Affect Disord 187:45–53.
13. Choi KS, Holtzheimer PE, Franco AR, Kelley ME, Dunlop BW, Hu XP, Mayberg HS (2014): Reconciling variable findings of white matter integrity in major depressive disorder. Neuropsychopharmacology 39:1332–1339.
14. Olvet DM, Delaparte L, Yeh F-CC, DeLorenzo C, McGrath PJ, Weissman MM, *et al.* (2016): A comprehensive examination of white matter tracts and connectometry in major depressive disorder. Depress Anxiety 33:56–65.
15. Ennis DB, Kindlmann G (2006): Orthogonal tensor invariants and the analysis of diffusion tensor magnetic resonance images. Magn Reson Med 55:136–146.

16. Alexander AL, Hurley SA, Samsonov AA, Adluru N, Hosseinbor AP, Mossahebi P, *et al.* (2011): Characterization of cerebral white matter properties using quantitative magnetic resonance imaging stains. Brain Connect 1:423–446.
17. Feldman HM, Yeatman JD, Lee ES, Barde LHF, Gaman-Bean S (2010): Diffusion tensor imaging: A review for pediatric researchers and clinicians. J Dev Behav Pediatr 31:346–356.
18. Soares JM, Marques P, Alves V, Sousa N (2013): A hitchhiker's guide to diffusion tensor imaging. Front Neurosci 7:31.
19. Jones DK, Knösche TR, Turner R (2013): White matter integrity, fiber count, and other fallacies: The do's and don'ts of diffusion MRI. NeuroImage 73:239–254.
20. Song SK, Sun SW, Ramsbottom MJ, Chang C, Russell J, Cross AH (2002): Dysmyelination revealed through MRI as increased radial (but unchanged axial) diffusion of water. NeuroImage 17:1429–1436.
21. Song SK, Yoshino J, Le TQ, Lin SJ, Sun SW, Cross AH, Armstrong RC (2005): Demyelination increases radial diffusivity in corpus callosum of mouse brain. Neuroimage 26:132–140.
22. De Santis S, Drakesmith M, Bells S, Assaf Y, Jones DK (2014): Why diffusion tensor MRI does well only some of the time: Variance and covariance of white matter tissue microstructure attributes in the living human brain. Neuroimage 89:35–44.
23. Song SK, Sun SW, Ju WK, Lin SJ, Cross AH, Neufeld AH (2003): Diffusion tensor imaging detects and differentiates axon and myelin degeneration in mouse optic nerve after retinal ischemia. Neuroimage 20:1714–1722.
24. Budde MD, Joong HK, Liang HF, Schmidt RE, Russell JH, Cross AH, Song SK (2007): Toward accurate diagnosis of white matter pathology using diffusion tensor imaging. Magn Reson Med 57:688–695.
25. Delorenzo C, Delaparte L, Thapa-Chhetry B, Miller JM, Mann JJ, Parsey RV (2013): Prediction of selective serotonin reuptake inhibitor response using diffusion-weighted MRI. Front Psychiatry 4:5.
26. Bracht T, Jones DK, Müller TJ, Wiest R, Walther S (2015): Limbic white matter microstructure plasticity reflects recovery from depression. J Affect Disord 170:143–149.
27. Korgaonkar MS, Williams LM, Ju Song Y, Usherwood T, Grieve SM (2014): Diffusion tensor imaging predictors of treatment outcomes in major depressive disorder. Br J Psychiatry 205:321–328.
28. Grieve SM, Korgaonkar MS, Gordon E, Williams LM, Rush AJ (2016): Prediction of nonremission to antidepressant therapy using diffusion tensor imaging. J Clin Psychiatry 77:e436–e443.
29. Lam RW, Milev R, Rotzinger S, Andreazza AC, Blier P, Brenner C, *et al.* (2016): Discovering biomarkers for antidepressant response: Protocol from the Canadian biomarker integration network in depression (CAN-BIND) and clinical characteristics of the first patient cohort. BMC Psychiatry 16:105.
30. MacQueen GM, Hassel S, Arnott SR, Addington J, Bowie CR, Bray SL, *et al.* (2019): The Canadian Biomarker Integration Network in Depression (CAN-BIND) magnetic resonance imaging protocols. J Psychiatry Neurosci 44:1–14.
31. Bell CC (2001): Diagnostic and Statistical Manual of Mental Disorders, Fourth Edition, Text Revision: DSM-IV-TR Quick Reference to the Diagnostic Criteria from DSM-IV-TR. JAMA 285:811–812.
32. Sheehan DV, Lecrubier Y, Sheehan KH, Amorim P, Janavs J, Weiller E, *et al.* (1998): The Mini-International Neuropsychiatric Interview (M.I.N.I.): The development and validation of a structured diagnostic psychiatric interview for DSM-IV and ICD-10. J Clin Psychiatry 59(suppl 20):22–23. quiz; 34–57.
33. Montgomery SA, Asberg M (1979): A new depression scale designed to be sensitive to change. Br J Psychiatry 134:382–389.
34. Mori S, Oishi K, Jiang H, Jiang L, Li X, Akhter K, *et al.* (2008): Stereotaxic white matter atlas based on diffusion tensor imaging in an ICBM template. Neuroimage 40:570–582.
35. Smith SM, Jenkinson M, Johansen-Berg H, Rueckert D, Nichols TE, Mackay CE, *et al.* (2006): Tract-based spatial statistics: Voxelwise analysis of multi-subject diffusion data. Neuroimage 31:1487–1505.
36. Jahanshad N, Kochunov PV, Sprooten E, Mandl RC, Nichols TE, Almasy L, *et al.* (2013): Multi-site genetic analysis of diffusion images and voxelwise heritability analysis: A pilot project of the ENIGMA-DTI working group. Neuroimage 81:455–469.
37. Kochunov P, Jahanshad N, Sprooten E, Nichols TE, Mandl RC, Almasy L, *et al.* (2014): Multi-site study of additive genetic effects on fractional anisotropy of cerebral white matter: Comparing meta and megaanalytical approaches for data pooling. Neuroimage 95:136–150.
38. Palacios EM, Martin AJ, Boss MA, Ezekiel F, Chang YS, Yuh EL, *et al.* (2017): Toward precision and reproducibility of diffusion tensor imaging: A multicenter diffusion phantom and traveling volunteer study. Am J Neuroradiol 38:537–545.
39. Davis AD (2018): CAN-BIND-DTI (v1.0) (Source code). Geneva, Switzerland: Zenodo.
40. Fortin JP, Parker D, Tunç B, Watanabe T, Elliott MA, Ruparel K, *et al.* (2017): Harmonization of multi-site diffusion tensor imaging data. Neuroimage 161:149–170.
41. Seabold S, Perktold J (2010): Statsmodels: Econometric and statistical modeling with python. Proc 9th Python Sci Conf 2010:57–61.
42. Galwey NW (2014): Introduction to Mixed Modelling: Beyond Regression and Analysis of Variance, 2nd ed. New York: Wiley.
43. Gumedze FN, Dunne TT (2011): Parameter estimation and inference in the linear mixed model. Linear Algebra Appl 435:1920–1944.
44. Shrout PE, Fleiss JL (1979): Intraclass correlations: Uses in assessing rater reliability. Psychol Bull 86:420–428.
45. Lakens D (2013): Calculating and reporting effect sizes to facilitate cumulative science: A practical primer for t-tests and ANOVAs. Front Psychol 4:863.
46. Wijtenburg SA, McGuire SA, Rowland LM, Sherman PM, Lancaster JL, Tate DF, *et al.* (2013): Relationship between fractional anisotropy of cerebral white matter and metabolite concentrations measured using 1H magnetic resonance spectroscopy in healthy adults. Neuroimage 66:161–168.
47. Portella MJ, de Diego-Adeliño J, Gómez-Ansón B, Morgan-Ferrando R, Vives Y, Puigdemont D, *et al.* (2011): Ventromedial prefrontal spectroscopic abnormalities over the course of depression: A comparison among first episode, remitted recurrent and chronic patients. J Psychiatr Res 45:427–434.
48. de Diego-Adeliño J, Portella M, Gómez-Ansón B, López-Moruelo O, Serra-Blasco M, Vives Y, *et al.* (2013): Hippocampal abnormalities of glutamate/glutamine, N-acetylaspartate and choline in patients with depression are related to past illness burden. J Psychiatry Neurosci 38:107–116.
49. Milne A, MacQueen GM, Yucel K, Soreni N, Hall GBC (2009): Hippocampal metabolic abnormalities at first onset and with recurrent episodes of a major depressive disorder: A proton magnetic resonance spectroscopy study. Neuroimage 47:36–41.
50. Braga RM, Buckner RL (2017): Parallel interdigitated distributed networks within the individual estimated by intrinsic functional connectivity. Neuron 95:457–471.e5.
51. Filley C (2012): The Behavioral Neurology of White Matter, 2nd ed. New York: Oxford University Press.
52. Lehéricy S, Ducros M, Moortele P-F Van De, Francois C, Thivard L, Poupon C, *et al.* (2004): Diffusion tensor fiber tracking shows distinct corticostriatal circuits in humans. Ann Neurol 55:522–529.
53. Wakana S, Jiang H, Nagae-Poetscher LM, van Zijl PCM, Mori S (2004): Fiber tract–based atlas of human white matter anatomy. Radiology 230:77–87.
54. Ota M, Noda T, Sato N, Hattori K, Hori H, Sasayama D, *et al.* (2015): White matter abnormalities in major depressive disorder with melancholic and atypical features: A diffusion tensor imaging study. Psychiatry Clin Neurosci 69:360–368.
55. Hyett MP, Perry A, Breakspear M, Wen W, Parker GB (2018): White matter alterations in the internal capsule and psychomotor impairment in melancholic depression. (L. Chao, editor) PLoS One 13:e0195672.
56. Parker G, Hadzi-Pavlovic D, Brodaty H, Boyce P, Mitchell P, Wilhelm K, *et al.* (1993): Psychomotor disturbance in depression: Defining the constructs. J Affect Disord 27:255–265.
57. Korgaonkar MS, Grieve SM, Koslow SH, Gabrieli JDE, Gordon E, Williams LM (2011): Loss of white matter integrity in major depressive

disorder: Evidence using tract-based spatial statistical analysis of diffusion tensor imaging. Hum Brain Mapp 32:2161–2171.
58. De Diego-Adeliño J, Pires P, Gómez-Ansón B, Serra-Blasco M, Vives-Gilabert Y, Puigdemont D, *et al.* (2014): Microstructural white-matter abnormalities associated with treatment resistance, severity and duration of illness in major depression. Psychol Med 44:1171–1182.
59. Schmahmann JD, Pandya DN (2009): Fiber Pathways of the Brain. New York: Oxford University Press.
60. Andrejević M, Meshi D, van den Bos W, Heekeren HR (2017): Individual differences in social desirability are associated with white-matter microstructure of the external capsule. Cogn Affect Behav Neurosci 17:1255–1264.
61. Hall GBC, Milne AMB, MacQueen GM (2013): An fMRI study of reward circuitry in patients with minimal or extensive history of major depression. Eur Arch Psychiatry Clin Neurosci 264:187–198.
62. Kieseppä T, Eerola M, Mäntylä R, Neuvonen T, Poutanen V-P, Luoma K, *et al.* (2010): Major depressive disorder and white matter abnormalities: A diffusion tensor imaging study with tract-based spatial statistics. J Affect Disord 120:240–244.
63. Petrides M, Pandya DN (2007): Efferent association pathways from the rostral prefrontal cortex in the macaque monkey. J Neurosci 27:11573–11586.
64. Schmahmann JD, Pandya DN, Wang R, Dai G, D'Arceuil HE, de Crespigny AJ, Wedeen VJ (2007): Association fibre pathways of the brain: Parallel observations from diffusion spectrum imaging and autoradiography. Brain 130:630–653.
65. de Schotten MT, Dell'Acqua F, Valabregue R, Catani M (2012): Monkey to human comparative anatomy of the frontal lobe association tracts. Cortex 48:82–96.
66. Heide RJ Von Der, Skipper LM, Klobusicky E, Olson IR (2013): Dissecting the uncinate fasciculus: Disorders, controversies and a hypothesis. Brain 136:1692–1707.
67. Hornberger M, Geng J, Hodges JR (2011): Convergent grey and white matter evidence of orbitofrontal cortex changes related to disinhibition in behavioural variant frontotemporal dementia. Brain 134:2502–2512.
68. Mincic AM (2015): Neuroanatomical correlates of negative emotionality-related traits: A systematic review and meta-analysis. Neuropsychologia 77:97–118.
69. Oishi K, Faria AV, van Zijl PCM, Mori S (2010): MRI Atlas of Human White Matter, 2nd ed. San Diego: Academic Press.
70. Cullen KR, Klimes-Dougan B, Muetzel R, Mueller BA, Camchong J, Houri A, *et al.* (2010): Altered white matter microstructure in adolescents with major depression: A preliminary study. J Am Acad Child Adolesc Psychiatry 49:173–183.e1.
71. Mayberg HS, Brannan SK, Mahurin RK, Jerabek PA, Brickman JS, Tekell JL, *et al.* (1997): Cingulate function in depression: A potential predictor of treatment response. Neuroreport 8:1057–1061.
72. Hunter JD (2007): Matplotlib: A 2D graphics environment. Comput Sci Eng 9:90–95.